LA-UR-19-23146
Approved for public release; distribution is unlimited.

Title: 2012 DREAM-HANE-RBR Summary Report

Author(s): Reeves, Geoffrey D.

Intended for: Report

Issued: 2019-04-08

Table of Contents

1. Overview of Tasks & Results (executive summary)

1.1 Technical Tasks

This report documents the results of a study to determine the efficacy of radiation belt remediation systems based on chemical releases in space. The major focus areas of this study were to:

1. improve the DREAM HANE model in order to better quantify the dose that a satellite would receive under a variety of burst scenarios
2. determine the whistler wave interaction with HANE electrons needed to effectively remediate the HANE dose
3. use numerical computer simulations to understand the production of whistler waves starting from an unstable ion ring distribution
4. conduct laboratory experiments to validate the numerical simulations and further quantify the production of whistler waves starting from an unstable ion ring distribution

1.2 Summary of Results

The primary results from each of these focus areas can be summarized as follows:

1. Substantial improvements to the DREAM HANE model were made. We made significant improvements in the Electron Source Model (ESM) which specifies the initial population of HANE electrons in the radiation belts as a function of yield and burst location. We developed an end-to-end capability in DREAM that allows us to calculate dose rates, from both natural and HANE radiation belts, as a function of time and position along an arbitrary satellite trajectory. We extended the physical model in the DREAM code from 1D (radial diffusion) to 3D (radial, energy, and pitch angle diffusion) which is required to capture energization and pitch angle scattering in addition to transport. This results were compared against an AFRL study done using the SNRTACS code providing higher confidence but also better insight into the strengths and limitations of each code. The full set of code development tasks was not completed due to higher priority on tasks 2-4 and early termination of the project.
2. We used the DREAM end-to-end model to evaluate the effect of whistler waves on a HANE electron population under several remediation scenarios. The calculation used realistic but somewhat simplified assumptions in order to meet project timelines. We found that the total HANE dose is highly sensitive to the natural processes that evolve the initial HANE source population at t=0 toward an equilibrium pitch angle distribution. This initial equilibration is not yet well-understood and is one factor that

emphasizes the need for pre-deployed satellite monitoring in any remediation system. In order to calculate the effectiveness of remediation we had to develop a quantitative metric which is further described in the report. We calculated the wave power needed (as a function of remediation duration) to meet the remediation target. This "reverse engineering" approach provides quantitative requirements for any remediation system that relies on VLF whistler waves.

3. We conducted a large number of simulations to understand production of whistler waves starting from an unstable ion ring distribution. We used super-computing scale Particle In Cell (PIC) simulations that fully, and self-consistently, capture the interaction of background plasma, unstable ring distributions, and the production and propagation of waves in the plasma. We studied the underlying scaling of the numerical simulations in order to understand how that scaling affects application to space plasma conditions and to laboratory plasma conditions. We developed a detailed understanding of the processes by which ring distributions decay to produce lower hybrid waves and the processes by which lower hybrid waves can be converted into whistler waves. We quantified the amount of energy converted in each step of the process and found it to be many orders of magnitude lower than calculated in previous studies.
4. In order to validate the simulations and give greater confidence to our conclusions we conducted experiments at the ULCL Large Area Plasma Device (LAPD) that replicated, as closely as possible, the physical processes captured in the simulations and in space. These experiments were conducted in three phases in order to understand each step in the chain of energy conversion. Careful and detailed measurements were taken at each phase in order to resolve ambiguities remaining from previous studies. Phase 1 involved the injection of lower hybrid waves using a low-power antenna in the LAPD and an artificial plasma depletion to simulate density striations. Phase 2 removed the artificial plasma depletion and increased the power on the antenna to the point where density striations were generated self-consistently. Phase 3 removed the antenna and injected an ion beam to produce an unstable ion ring distribution as the source for lower hybrid waves. In each phase we made measurements to identify whistler waves and to measure their amplitude and propagation. As with the simulations, only a very small fraction of the lower hybrid wave energy was converted to energy in the propagating whistler waves. We found the results of the experiments and the simulations to be in good agreement which gives us more confidence in applying the results to conditions in space than we would have had from either simulations or experiments alone.

2. Radiation Belt Remediation (RBR)

2.1 Introduction

This section is intended as an overview of the general problem for readers that are not as familiar with radiation belt physics, the origin and characteristics of nuclear-generated radiation belts, or the characteristics of the Earth's magnetic and radiation environments. These are all factors that affect calculations of risk to satellites and calculations of the effectiveness of radiation belt remediation (RBR) systems. A discussion of chemical release RBR systems begins at section 2.2. A discussion of the specific results of our study begins at section 3.

2.1.1 The Natural Radiation Belts

To better understand the contents of this report and the physical basis behind radiation belt remediation systems it is helpful to include a basic description of the natural radiation belts. This section also introduces and defines some terminology that is used elsewhere in the report.

The Earth's radiation belts are composed of energetic electrons (and ions) that are trapped in the Earth's magnetic field (also called the geomagnetic field). The energies of electrons that are considered part of the radiation belt population are much higher than the thermal energy of the bulk of the plasma. While there is no precise definition electrons with energies greater than about 500 keV (0.5 MeV) are considered "radiation belt" electrons. They are also referred to as "relativistic electrons" because their energy is comparable to or larger than the rest mass energy (0.511 MeV).

Electrons in the natural radiation belts come from lower-energy electrons that are accelerated to MeV energies. The processes for acceleration are still the subject of research [*Friedel et al.*, 2002] but the most recent theories suggest that they are accelerated by interaction with electromagnetic waves in the magnetosphere [*Summers et al.*, 1998; *Reeves et al.*, 2009]. Similar interactions with electromagnetic waves scatter electrons by changing their pitch angle (the angle between the velocity vector and the magnetic field measured at magnetic equator - i.e. the minimum B point on a magnetic field line). Electrons with equatorial pitch angles near 90° stay trapped near the magnetic equator while electrons with equatorial pitch angles near 0° or 180° have velocity vectors very close to the magnetic field direction and will travel along the field until they hit the atmosphere where they are absorbed. The absorption of electrons in the atmosphere and loss from the system is referred to as "electron precipitation". The objective of radiation belt remediation is to increase the rate of electron precipitation and thereby remove more electrons from the radiation belts and decrease the risk they pose to satellites.

Electrons trapped in the geomagnetic field undergo three periodic motions that are important to understand in the context of radiation belt remediation (Figure 2.1). The first is gyration around a magnetic field line. The second is "bounce" motion back and forth along a magnetic field line between magnetic mirror points. The third is azimuthal (longitudinal) motion around the Earth along the magnetic drift shell. Because of these motions it is convenient to label the entire population of electrons on a given drift shell by the parameter L which is defined as the geocentric distance to the equatorial point on a given field line (or drift shell). L is measured in Earth radii (R_E) where 1 R_E = 6370 km. For this reason "drift shells" are typically referred to as L-shells and will be in this report.

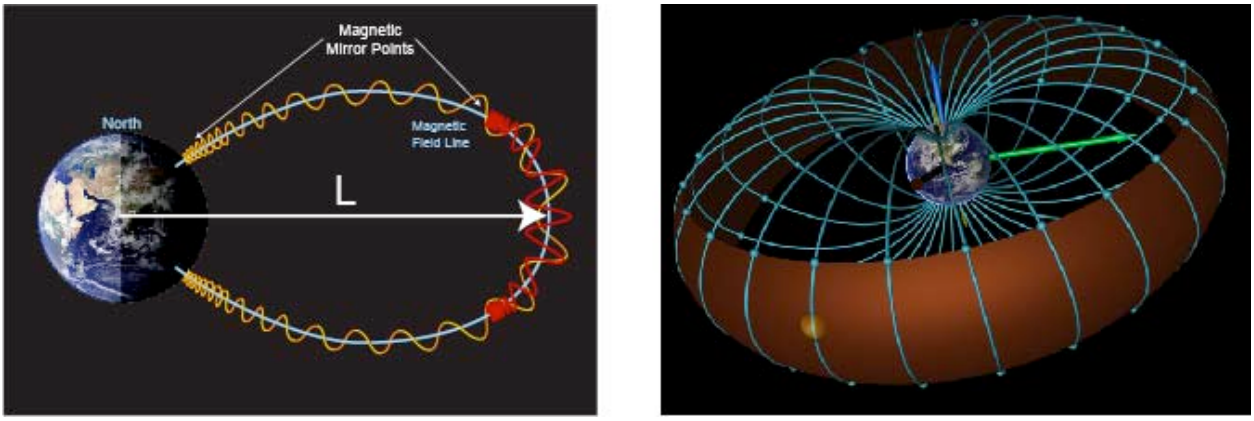

Figure 2.1: Illustration of the motion of electrons in the radiation belts.

The Earth's surface is at L=1. Geosynchronous orbit is at L=6.6. The outer electron belt spans approximately L=3-8 and is highly dynamic, responding to solar and geomagnetic activity. The inner electron belt spans approximately L=1-2 where electrons are very stable and remain trapped for very long times. The two belts are separated by a "slot" region at L≈2-3 where natural electron fluxes are typically low. Figure 2.2 shows the average intensity of 2 MeV electrons in the electron belts. Red represents 10^6 electrons/cm^2/s, yellow represents 10^3 electrons/cm^2/s and violet represents ~1 electron/cm^2/s

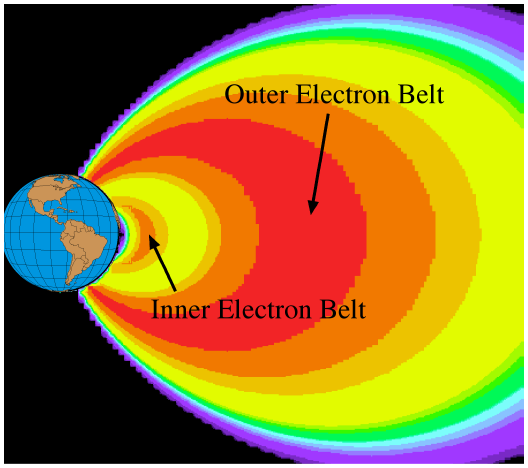

Figure 2.2: Average structure of the natural Van Allen radiation belts.

It's clear that the average intensity of the radiation belts can vary by many orders of magnitude depending on the location in space (the L-shell). Figure 2.2 also shows that the radiation belts extend along the magnetic field lines down to the Earth's atmosphere. Even low-earth-orbiting (LEO) satellites encounter the radiation belts. Similarly, as discussed below, a nuclear explosion will produce a population of electrons that extend along the magnetic field lines far out into space regardless of the altitude of the explosion.

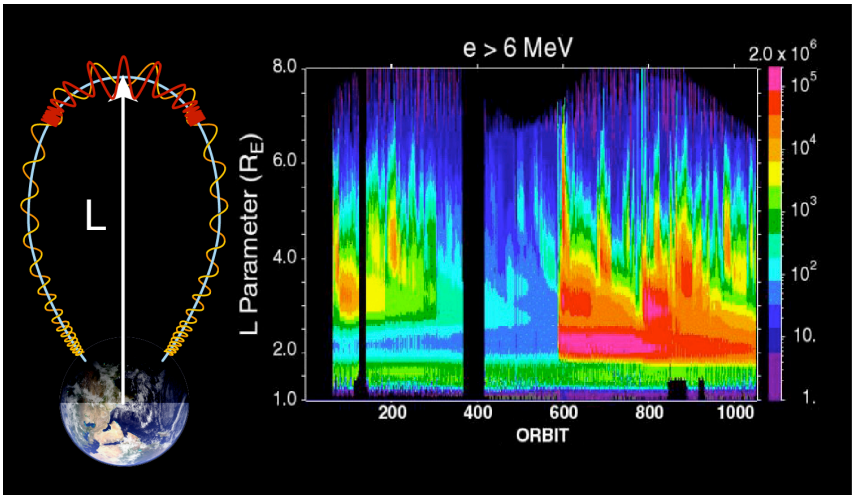

Figure 2.3: Illustration of the meaning of the "L" parameter and a plot of radiation belt intensity as a function of L and time.

In addition to the spatial variation seen in figure 2.2, the natural radiation belts also vary greatly in time. Figure 2.3 shows electron fluxes measured by the CRRES satellite as a function of L-shell and time (with the definition of L as a reminder). This figure shows that, even at a fixed point in space, the electron flux can also vary by many orders of magnitude. The abrupt increase near orbit 600 (March 1991) occurred in minutes and filled what is normally the slot region [*Blake et al.*, 1992]. In many ways this natural event simulates the effects of a high altitude nuclear explosion and provides a natural laboratory for testing theories. Figure 2.3 also shows times when the electron intensity drops suddenly by many orders of magnitude. These electron precipitation events are also subject of ongoing research [*Millan and Thorne*, 2007] but are not fully understood. Radiation belt remediation systems must exploit whatever processes produce these losses but enhance the loss rates and target them to specific regions of space.

2.1.2 Belts from High Altitude Nuclear Explosions (HANE)

Exoatmospheric nuclear explosions produce "artificial" radiation belts that pose a much greater threat to satellites than the natural belts. A high altitude nuclear explosion, HANE (or "detonation" - HAND) produces a large number of radioactive debris ions. Those ions

beta decay to produce MeV electrons. The subsequent HANE electron belt is very similar to the natural electron belts but is much more intense and much more narrowly-confined in L-shell. The HANE electrons also gyrate, bounce, and drift around the Earth to produce a "shell" of electrons (see figure 2.1). Figure 2.4 shows a cut-away view of the radiation belts with the inner electron belt removed to show the location and extent of the HANE belt assuming a detonation over Korea.

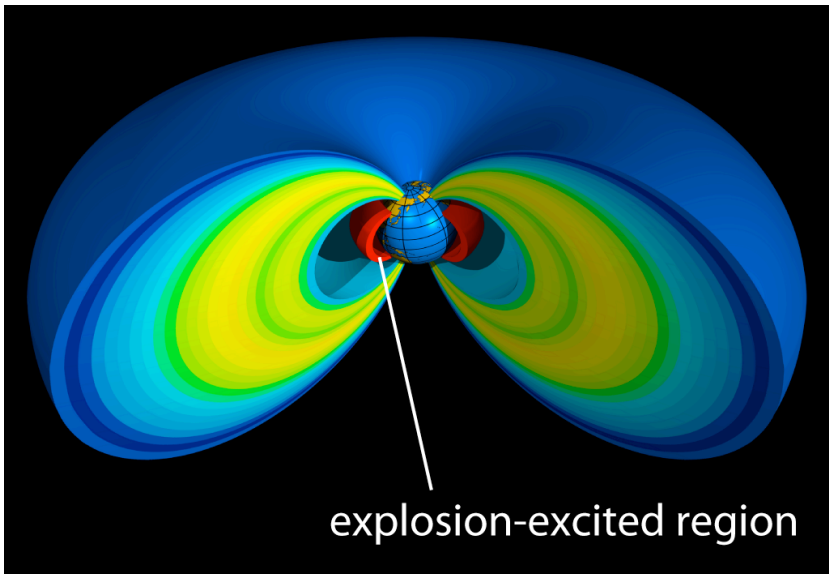

Figure 2.4: Illustration of a HANE belt at low L-shells.

The intensity of a HANE belt is primarily controlled by the yield of the device. The number of debris ions and beta-decay electrons scale linearly with the yield. The debris ions very quickly decay and become charge-neutralized so it is the long-lasting electrons that pose the greatest threat to satellites. The intensity of the belt at a specific point in space is given by the total number of electrons divided by the volume of space that the belt occupies.

The spatial extent of a HANE radiation belt is determined by two factors. The first factor is the geographic location of the explosion. Explosions at low geographic latitude, such as Starfish, will populate L-shells very close to the Earth ($L \approx 1$). Explosions at high geographic latitudes will populate high L-shells. An explosion over Fairbanks, Alaska would produce a HANE belt at $L \approx 6.6$ which is the L-shell where geosynchronous satellites operate. The second factor is the radial extent (i.e. ΔL). ΔL is controlled by the size of the diamagnetic cavity produced in the initial blast. If the explosion is at relatively low altitude ($h<1000$ km) then ΔL is relatively small ($\Delta L<0.3$) and the HANE belt is narrowly confined.

The location and spatial extent of the HANE belt is an extremely important parameter for assessing the impact to satellites. The dose from a HANE belt to a given satellite is a function of the intensity of the belt and the amount of time that a particular satellite spends in that belt which, in turn, is a function of the orbit. LEO satellites are generally considered

to be at the highest risk from a HANE belt. Any satellite with an inclination greater than the geographic latitude of the burst will encounter the HANE belt four times per orbit (north and south on both the ascending and descending legs).

The threat to a given satellite is a function of a number of parameters including yield, latitude, longitude, altitude etc. Therefore any quantitative assessment of risk has to be parametric and has to include assumptions that limit the total number of risk cases. For our study we assumed that the HANE belt populates L<2 because this is the region where the lifetime of the electrons is longest and therefore poses the greatest risk. This assumption still includes a very large range of scenarios as the geographic region that maps to L<2 still covers most of the populated surface of the globe (figure 2.5).

The relationship between L and geographic latitude is not constant with longitude due to the complex asymmetry of the magnetic field close to the Earth's surface (i.e. the non-dipole components). This is the same effect the produces the South Atlantic Anomaly (SAA), The asymmetry of the magnetic field that produces the SAA also affects the geographic distribution of HANE electrons at a particular satellite altitude. It is an additional complication that must (a) be taken into account when calculating dose to a satellite and (b) carefully accounted for when calculating the electron loss by precipitation into the atmosphere by either natural processes or by remediation systems.

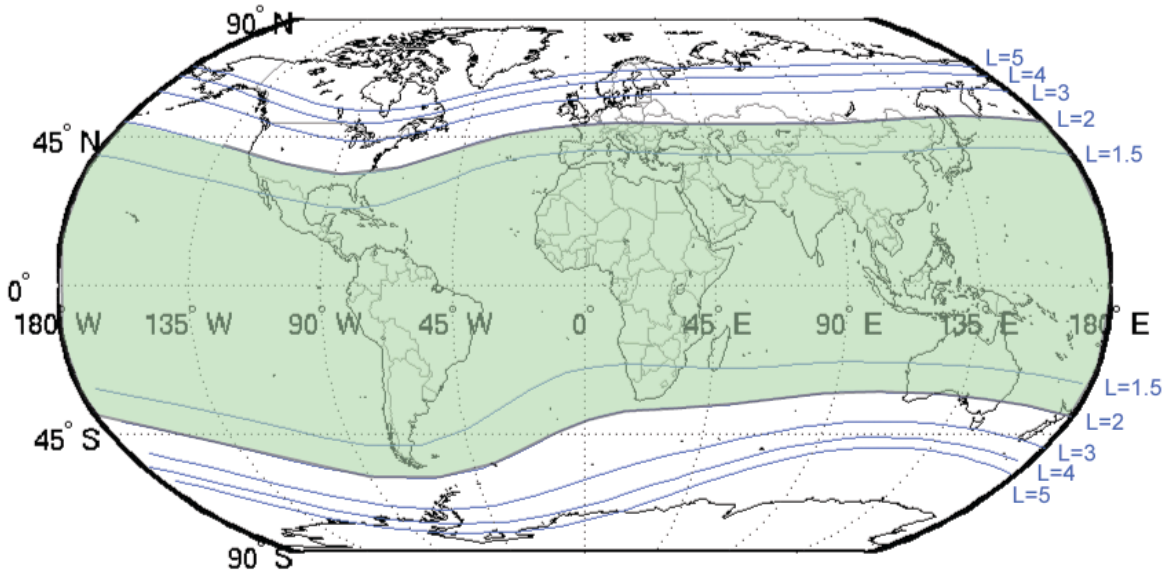

Figure 2.5: The extent of the region L<2 mapped to the upper atmosphere. Asymmetries are caused by the Earth's non-dipole magnetic field.

2.1.3 General Remediation Issues

In order to precipitate into the atmosphere, an electron must mirror at a low enough altitude that it gets absorbed by the neutral gas in the atmosphere. The point at which an electron mirrors on a magnetic field line (see figure 2.1) is given by it's equatorial pitch angle and the strength of the magnetic field. Specifically

$$\frac{B_{eq}}{B_m} = \sin^2 \alpha$$

where B_{eq} is the magnetic field strength at the equator, B_m is the field strength at the mirror point and α is the electron equatorial pitch angle.

The height of the mirror point, H_m is a function of the strength of the magnetic field which decreases with altitude along a given magnetic field line. Lower H_m = Larger B_m. In order to lower the mirror altitude below the nominal "top" of the atmosphere (~100 km) a remediation system has to change an electron's pitch angle by some form of scattering. The range of pitch angles for which the mirror altitude is below the top of the atmosphere is called the "loss cone" (figure 2.6). The objective of a remediation system is to scatter an electron into this loss cone either through large-angle scattering or many small small angle scatters (diffusion). For example, if the loss cone is 10° wide then all electrons with pitch angles $10° < \alpha < 90°$ must be scattered such that $\alpha < 10°$ in order to be lost.

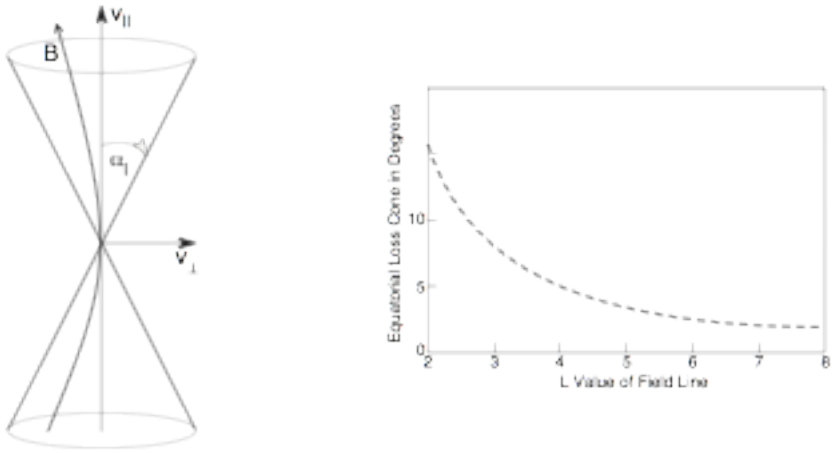

Figure 2.6. An illustration that defines pitch angle and a plot of the size of the atmospheric loss cone as a function of L.

Two processes that can change an electron's pitch angle are Coulomb scattering and resonant scattering by electromagnetic waves. Coulomb scattering occurs when an electron's velocity is perturbed by a DC electric field either from electrostatic structures

(i.e. charged tethers) or by electrically charged materials (e.g molecular ions, metallic dust, etc.)

Resonant wave-particle scattering occurs when an electron encounters a wave whose electric field component rotates around the magnetic field at the same rate that the electron gyrates around the filed. The electron experiences a constant electric field for long enough to change it's velocity vector and hence it's pitch angle. For radiation belt electrons the frequency of resonant waves are in the VLF band and, in a magnetized plasma, VLF electromagnetic waves can come in a variety of forms including whistler waves, lower hybrid waves, ion cyclotron waves, and magnetosonic waves. The properties of these different wave forms makes them interact differently with radiation belt electrons. For electrons with MeV energies (including HANE electrons) it is whistler waves that produce the most effective scattering and can best be exploited for RBR. Whistler waves can be produced by a number of means including ground transmitters, space transmitters, modulated low-energy electron beams in space, chemical releases in space, or changes to the ambient plasma distributions.

The volume of the HANE belt that needs to be remediated is a 3-dimensional volume that encircles the Earth, covers a range of L-shells (ΔL), and extends the full length of the field from hemisphere to hemisphere. It is not feasible to deploy a remediation system that spans that entire volume (millions of cubic kilometers). Rather RBR systems exploit the azimuthal drift of radiation belt electrons. The magnetic forces that constrain electron motion (bouncing between magnetic mirror points) also impart an azimuthal (longitudinal) velocity called the drift velocity. An electron with an energy of 1 MeV at L=2 has a drift velocity that allows it to circle the Earth in about 1 hour. A remediation system can then still be effective if it fills a limited volume of space but exploits the drift of the electrons to bring them into the effective area.

Pitch angle scattering can occur anywhere along the magnetic field line but losses only occur when the pitch angle moves across the critical boundary between mirror points above the atmosphere (i.e. trapped) to below the atmosphere (i.e. in the loss cone). Scattering that occurs near the top of the atmosphere only needs to change the pitch angle a little (e.g. from 11° to 9°) while scattering at higher altitude needs to produce a larger change in pitch angle. Ultimately, to remove all electrons from a HANE belt they all have to scatter into the loss cone but a system that operates continuously at low altitudes can provide a LEO "safe zone" provided it scatters electrons faster than the natural scattering replenishes them from above.

2.2 Chemical Release Remediation

Our investigation focused on radiation belt remediation through electron scattering by electromagnetic whistler waves produced by a chemical release in space. We refer to this here as Chemical Release Remediation. The remediation scheme is extremely simple conceptually but actually relies on a complex chain of processes that lie between the

initial action (chemical release) and the desired end effect (HANE electron precipitation). In the simplest terms the steps are to release a material (chemical) that ionizes and interacts with the plasma to produce electromagnetic whistler waves that then scatter the electrons into the atmosphere.

A more detailed accounting of the processes can be described as follows:

1. Release a sufficient quantity of material with a sufficient energy.
2. The material photo-ionizes when it is in sunlight.
3. The newly-ionized material is now trapped on the magnetic field lines and gyrates around the magnetic field (like the electrons do) to form an “ion ring distribution”.
4. Ion ring distributions are unstable and their energy is quickly converted into lower-hybrid waves and thermal heating of the background plasma.
5. Lower hybrid waves interact only weakly with radiation belt electrons but some of the energy may be converted to whistler waves through non-linear processes.
6. Whistler waves propagate away from the release region where they can interact with HANE electrons.
7. HANE electrons are scattered into the atmospheric loss cone and removed from the system.

Our study, described here, begins with step 4. We start by assuming that an ion ring distribution exists in space and follow the chain of processes that ultimately leads to scattering of radiation belt electrons into the atmosphere. In particular we studied step 5 in great detail. The conversion of one type of plasma wave into another type is a non-linear process in which only a fraction of the energy is converted. Therefore knowing the conversion efficiency is critical to quantifying what constitutes a “sufficient quantity of material with sufficient energy”.

3. LANL Study Results

3.1 Introduction to the LANL studies

We adopted a two-pronged approach to investigating the production of whistler waves from an initial ion ring distribution. The first approach was to use numerical simulations - specifically and the second was to reproduce the same conditions as closely as possible in the laboratory. The objectives of both were to determine how much of the energy in the initial ring distribution ended up as energy in whistler waves. We refer to this as the conversion efficiency, ε. The conversion is actually a two-step process. First conversion of ring energy to energy in lower hybrid waves which has an efficiency ε_{LH} and second,

conversion of lower hybrid waves into whistler waves which has an efficiency ε_W. The ring-to-whistler conversion efficiency is a product of the two: $\varepsilon = \varepsilon_{LH} \times \varepsilon_W$ so each step must be relatively efficient to get a large total efficiency.

Numerical particle-in-cell (PIC) simulations have several characteristics that make them ideal for this problem. Unlike conventional analytic theory they do not require a complex theory or any underlying assumptions about the equations. PIC simulations follow each electron and each ion and their interactions with each other according to Maxwell's equations. Essentially, you set up the initial conditions, let it run, and analyze the results. The primary disadvantage is that a huge number of particles has to be tracked and a mind-boggling number of calculations need to be done by the computer. The PIC simulations needed for solving our problem have only recently been feasible with the development of "petaflop computing". A petaflop computer is capable of performing 10^{15} floating point operations per second (flop).

We conducted laboratory experiments using the Large Area Plasma Device (LAPD) at UCLA. The objective of the laboratory experiments was to verify that the PIC simulation results could be reproduced, to study wave conversion in a realistic environment, and to understand how the results of both the simulation and the experiments should be scaled to the conditions in space. We conducted three types of experiments. The first used an antenna to inject lower hybrid waves directly into the plasma at moderate powers. The second used the same direct injection but studied the response as a function of injected power. The third did not use and antenna. It used an ion beam from an accelerator to produce an ion ring distribution.

Previous studies found that the conversion efficiency of ion ring energy to lower hybrid waves to whistler waves, ε, was about 10% which is just sufficient to make a chemical release remediation system feasible. Our results from both the PIC simulations and laboratory experiments showed that $\varepsilon \approx 10^{-5}$ which puts the amount of chemical required well outside of practical limits. Results of the PIC simulations and laboratory experiments are presented in sections 3.2 and 3.3.

Earlier studies also assumed that the whistler waves would propagate over a large volume of the magnetosphere and produce loss of 100% of the HANE electrons in that volume. Our studies showed that the whistler waves propagate nearly parallel to the magnetic field and therefore cover only a limited volume of space. This means that deployment of a remediation system needs to be in the HANE belt itself. We also conducted more detailed calculations of the pitch angle scattering as a function of time without assuming 100% loss. This gives us very reliable estimates of the amount of whistler power as a function of time that is needed to remediate a HANE belt - regardless of the source of those whistler waves. We call this the "reverse engineering" problem and the results are presented in section 3.4.

The other question that needs to be answered is; How intense is the HANE belt? In other words: What needs to be remediated? As discussed above, the intensity and location of

the HANE belt in space is a function of device yield and the location of the detonation. Section 3.5 describes our HANE electron source model and some studies of the dependence of the HANE belt on those initial conditions.

3.2 Summary of Results from the Numerical Simulations

A primary objective of our study was to use large-scale numerical simulations to investigate the conversion of energy in an unstable ion ring distribution to lower hybrid waves and subsequent nonlinear conversion of the lower hybrid waves into whistler waves.

There are three general classes of numerical simulations of plasmas: fluid, hybrid, and particle-in-cell (PIC). Fluid simulations treat both the ions and electrons in the plasma as fluids. Hybrid simulations treat the ions as particles but the electrons as a fluid. PIC simulations treat both the electrons and the ions as particles and solve the full equations of motion (Maxwell's Equations) for the charged plasma particles and the electromagnetic fields. Therefore only PIC simulations are suitable for the problem at hand.

PIC simulations are powerful but are also limited by the very large number of calculations that must be performed. PIC simulations put limits on the simulations that make them feasible. As computers have gotten more powerful the limits that must be placed on PIC simulations to make them tractable have relaxed but they have not disappeared. Therefore, we put a considerable amount of work into performing different simulations with different numerical conditions to ensure the results are robust and not limited to a specific set of assumptions. (The dependence of our numerical results on these assumptions will also be discussed below.)

Another important point to understand in numerical plasma simulations is the use of "dimensionless units". Characteristic lengths and times can vary over many orders of magnitude depending on the conditions in the plasma (temperature, density, etc.) but, as conditions are varied, many of the important parameters scale together. Therefore, to simulate a wide range of conditions time is not expressed in seconds but rather by the number of periods of characteristic oscillations in the plasma. For example, the electron plasma frequency is a characteristic frequency in all plasmas and is defined as $\omega_{pe} = (4\pi ne^2/m_e)^{1/2}$ where n = electron density, e = electron charge, and m_e = electron mass. Similarly there is an ion plasma frequency ω_{pi}. Time can be expressed dimensionlessly (without units) as, for example, the quantity $t\,\omega_{pi}$ which is then independent of the plasma density or the electron/ion mass ratio chosen for the simulation. When quantitative results are given (e.g. for energy conversion efficiencies) we "plug in" the appropriate numbers and calculate the quantities in physical units.

3.2.1 Calculation of the Conversion Efficiency

The initial "free energy" that is the source of all waves in the system is the kinetic energy in the unstable plasma ion ring distribution. Using m_r as the mass of the ions in the ring distribution (the mass of the release chemical) and V_r as the velocity of the ring ions (perpendicular to the magnetic field, the kinetic energy of a ring ion, $E_r = ½m_rV_r^2$. The total energy will be proportional to the number of ions, N_r.The number of ions is equal to the density of the ring ions, n_r, times the volume, V. Thus the total energy in the ring plasma is N_rE_rV.

For remediation applications we are ultimately interested in the amount of energy that propagates away from the release region and is available to scatter radiation belt electrons. The energy in any non-propagating waves (such as the electrostatic component of the lower hybrid waves) stays local and ultimately dissipates its energy by heating the local plasma. The energy in a propagating plasma wave is proportional to the magnetic component of the wave, $E_w = \delta B_w^2/8\pi$ and the total energy is obtained by integrating over the volume, $V(\delta B_w^2/8\pi)$.

In this section we give the "bottom line" estimate of the conversion efficiency of ring energy to whistler energy and in the following section we discuss the results of the simulations in more detail.

The quantitative estimate of the conversion efficiency, ε, is derived here using a combination of results from the numerical simulations and from plasma theory. The detailed steps in calculating the efficiency are given in Appendix B of this report.

The efficiency, ε, is the total amount of whistler wave power divided by the total amount of energy in the ring distribution so,

$$\varepsilon = \frac{V\left|\partial B_W^2\right|/8\pi}{Vn_rE_r}$$

This is not a quantity that can be directly pulled out of the numerical simulations but it can be calculated based on ratios of quantities that are either readily available from the simulations or can be calculated through analytic theory. (A detailed description of analytic theory is given in Appendix A which includes a review of previous studies along with a description of the methods that we used.)

We can turn the efficiency equation into a form that can be more directly calculated by multiplying the numerator and denominator by $\delta E_{ES}^2\, n_0T_i$. Here E_{ES} is the "electrostatic" amplitude of the lower hybrid waves and n_0T_i is the density and temperature of the background plasma ions. The maximum amplitude of the electrostatic amplitude (the saturation amplitude) obtained from the simulations is nearly identical to that derived from analytic theory so we use the analytic values and designate them by (th). The efficiency equation then becomes

$$\varepsilon = \frac{\left|\partial B_W^2\right|/8\pi}{n_r E_r} = \left(\frac{\left|\partial B_W^2\right|}{\left|\partial E_{ES}^2(th)\right|}\right)\left(\frac{\left|\partial E_{ES}^2(th)\right|/8\pi}{n_0 T_i}\right)\left(\frac{n_0 T_i}{n_r E_r}\right)$$

The first term is the ratio of magnetic power in the whistler waves to electrostatic power in the lower hybrid waves which can be directly determined from the simulations as discussed in Part 3 of the simulation report. As discussed in Appendix B, wave-wave conversion requires that both the frequency and wave normal components of the whistler and lower hybrid waves match so, in the simulations, they are in essence part of one overall fluctuation and cannot be unambiguously separated. However, the electric field fluctuations are dominated by the lower hybrid wave and the magnetic field fluctuations are dominated by the whistler wave. So, in the simulations we take a "best case" scenario and use the maximum amplitude of the electric field fluctuations as the lower hybrid power and the maximum amplitude of the magnetic field fluctuations as the whistler power. This gives a "best case" estimate of the ratio of whistler power to lower hybrid power of about 10%.

Part 3 of the numerical simulation report applies further analysis to derive a "scaling law" for the conversion efficiency that can be applied to specific scenarios in the laboratory or in the magnetosphere. A scaling law determines the basic plasma parameters (or ratios) that control the physical processes. Once those parameters have been determined the efficiency can be expressed as a constant factor times the scaling parameters and only the scaling parameters vary from one physical environment to another.

As shown in Part 3 the efficiency equation can be expressed as a function of 4 scaling parameters:

(v_r/v_{th}) which is the ratio of the velocity of the ring ions to the thermal velocity of the background ions,

(n_r/n_0) which is the ratio of the ring ion density to the background ion density,

(m_r/m_i) which is the ratio of the ring ion mass to background ion mass, and

β which is the ratio of the plasma particle pressure to the magnetic field pressure.

The scaling law is then

$$\varepsilon \approx 8\times 10^{-4}\, f\beta_i \left(\frac{v_r}{v_{th}}\right)^2 \left(\frac{n_r}{n_0}\right)^{-2/5} \left(\frac{m_r}{m_i}\right)^{-3/5}$$

The factor $8 \times 10^{-4} f$ is a constant and f is a factor that arises from corrections to cold plasma approximations needed when the plasma is warm - as it is in the magnetosphere.

For a chemical release in the magnetosphere we can plug in the appropriate values:

$\beta = 2.5 \times 10^{-5}$

$(v_r/v_{th}) = 5$

$(n_r/n_0) = 0.2$

$(m_r/m_i) = 8.6$

With the warm plasma factor $f = 0.4$ we get

$$\varepsilon \approx 8\times 10^{-4}(0.4)(2.5\times 10^{-5})(5)^2(0.2)^{-2/5}(8.6)^{-3/5} \approx 1\times 10^{-7}$$

The detailed steps in this calculation are shown in detail in Part 3 of the numerical simulation report. Part 3 also relates this calculated efficiency to efficiencies calculated by other means in order to assess the quantitative agreement between analytic theory, numerical simulations, the scaling law above (based on a combination of simulation and theory), and previous estimates using nonlinear theory [e.g. *Mithaiwala et al.*, 2011]. The results are summarized in the table below and discussed in detail in the numerical simulation report, Part 3. The labels in quotes are the ones used in table 1 of Part 3. One reason that we have confidence in our estimate of the efficiency is the remarkably close agreement that we obtain through three different approaches to calculating the energy partitioning. We note, however, that the results are vastly different than those previously calculated using nonlinear theory which uses both a different mathematical approach and quite different physical assumptions (as is also discussed in Part 3 of the numerical simulations report).

	Analytic Theory "LHPPW"	**Numerical Simulation "Sim"**	**Scaling Law** (analytic + sim) **"Scaling"**	**Nonlinear Theory "NLWPS"**
change in ring energy, ΔE_r	-0.04	-0.04	-0.07	-0.1
heating of background ions, ΔEi	0.025	0.025	0.037	0.0
heating of background electrons, ΔEe	0.015	0.015	0.033	0.0

	Analytic Theory "LHPPW"	**Numerical Simulation "Sim"**	**Scaling Law** (analytic + sim) **"Scaling"**	**Nonlinear Theory "NLWPS"**
Electrostatic (lower hybrid) Fluctuations, $\|\delta E_{ES}^2\|$	5×10^{-3}	3×10^{-4}	3×10^{-3}	8×10^{-7}
Magnetic (whistler) Fluctuations, $\|\delta B_w^2\|$	8×10^{-5}	8×10^{-5}	7×10^{-5}	1×10^{-1}
lower hybrid growth rate, $\gamma_{LH}\tau$	5	7	5	6000

Table 3.2.1 Important quantities calculated using different techniques. Calculations using Analytic Theory, Numerical Simulation, and a hybrid approach (Scaling law) all provide very similar values.

3.2.2 Conversion Efficiency as a function of Simulation Parameters

Numerical Particle In Cell (PIC) simulations are a powerful tool for studying both linear and nonlinear processes in plasmas. No simplifying physical assumptions need to be made. Rather, the simulation is set up with an initial condition and then just runs. PIC simulations do, however, have other limitations stemming from the very large number of calculations that need to be done. It is not possible, even with the most modern computers, to simulate the exact conditions in the magnetosphere. The spatial dimensions and number of particles are simply too large. Therefore all PIC simulations apply numerical limits that need to be considered when interpreting the results. Therefore another big task in our work was to study how the results of the simulations might vary under different numerical limits.

Typical limits include:

1. The number of particles in the simulation.

2. The resolution of the numerical grid used in the simulations - e.g. the size (or resolution) of the discrete steps used in each parameter (length, energy, etc.).

3. The physical length of each dimension in the simulation. The larger the dimensions the more calculations need to be done but dimensions must be large enough to capture the dynamics of the system. Dynamics can include particle motion or the characteristic wavelength of wave of interest. In our simulations we required that the dimensions be much larger than the wavelength of lower hybrid and of whistler waves.

4. The number of dimensions used in the simulation. Simulations can be done in reduced dimensions. A problem that is completely uniform in the x-y directions can be calculated only as a function of z. Problems with cylindrical symmetry such as parallel or perpendicular to a magnetic field can be done in 2 dimensions. Or, in the most realistic and computationally intensive case, all three dimensions can be simulated numerically. We performed both 2-dimensional and 3-dimensional simulations.

5.) Using electrostatic approximations. For cases where electromagnetic waves are not important, simulations can ignore all but the background (imposed) magnetic field. Lower hybrid waves are, for example, very nearly electrostatic and their growth from ion ring distributions can be calculated using electrostatic simulations. Whistler waves, on the other hand are electromagnetic so the conversion of lower hybrid to whistler waves must be done using a fully electromagnetic code.

6. The electron/ion mass ratios. The number of calculations needed scales with the number of time steps in the simulations. Time steps must be short enough to resolve the motion of all the particles. Since the electron mass is much lower than the proton mass ($m_p/m_e \approx 1836$) ions move much slower than electrons. In order to make the number of time steps needed to resolve electron motion closer to that for ions, PIC simulations assume an artificial mass ratio closer to 1. For many problems this simplification has no effect but for our problem we used a range of mass ratios in order to understand how the results scale with that assumption.

The numerical limits of the simulations and the use of dimensionless units in the simulations makes the calculations feasible but can make the results difficult for non-experts to interpret. One must also be careful in applying the results to the actual conditions in a given plasma system and understanding how the physical processes scale from one set of plasma parameters to another. This detailed analysis is presented in Parts 1-3 of the numerical simulation report along with the three Appendices A-C. This was also part of the motivation for conducting laboratory experiments to reproduce the same energy and wave-wave conversion processes. The results of the laboratory experiments are described in section 3.2 of this report an in the attached laboratory experiments report.

Part 1 of the numerical simulations report examines the dependence on the plasma parameter β which is a fundamental parameter that controls waves in plasmas. In a magnetically confined plasma, $\beta < 1$. In fusion plasmas or the solar corona β can be of order 0.1 but in the low-altitude magnetosphere $\beta \approx 10^{-5}$. Part 1 describes simulations with two PIC codes, NPIC and VPIC for low β (= 0.006), and high β (= 0.06) as well as

electrostatic simulations with $\beta = 0$. The results showed that the growth of lower hybrid waves from an ion ring distribution is very well understood and that 3D electromagnetic simulations are in very close agreement to earlier simplified calculations that assume 2 dimensions or use an electrostatic approximation. They are also in close agreement to quasi-linear analytic theory. The dependence of the lower hybrid waves on β is also straight-forward. For β=0 the lower hybrid waves are purely electrostatic - the energy in the magnetic components ($|\delta B_{LH}^{2}|$) is zero, and the waves have a wave normal direction ($\mathbf{k}$) exactly perpendicular to the background field, B, so $k = k_{\perp}$ and $k_{||} = 0$. For low β there is a small magnetic component to the wave that increases as β increases making the wave more electromagnetic $\delta B_{LH}^{2} \neq 0$ and more oblique, $k_{||} \neq 0$. In contrast, the conversion from lower hybrid to whistler waves was a more complex function of the plasma and numerical parameters as discussed below.

Part 3 describes simulations that examine the dependence on the assumed electron to ion mass ratio and the dimensionality of the simulation. Both 2-D and 3-D simulations were carried out using the same initial conditions and parameters as in Part 1, but keeping the background plasma beta fixed at $\beta = 0.006$, and instead varying the mass ratio of the background ions to electrons, m_i/m_e. When properly normalized to the lower hybrid frequency (ω_{LH}) or to the ion plasma frequency (ω_{pi}), the properties of the lower hybrid waves are essentially independent of m_i/m_e, consistent with linear theory and simple nonlinear arguments. However, the conversion to whistler waves is strongly dependent on the mass ratio as well as the geometry of the simulations (being much stronger in 2-D than in 3-D). Part 2 includes a single high β (= 0.06) simulation at high mass ratio (mi/me = 1024) to compare with the results in Part 1. Part 2 also describes some numerical experiments that we have done to compare similarities and differences in the results that arise from using different simulation codes, numerical parameters and computer systems.

Part 3 of the numerical simulation report presents an overview of the conversion of lower hybrid waves to whistler waves. It presents the results from theory and from our numerical simulations. It also details the quantitative calculation of the energy conversion efficiencies. Part 3 includes details of the calculations summarized in section 3.2.1 above.

Figure 3.2.1 shows a standard diagnostic plot for the numerical simulations. The plots show the wave growth as a function of (dimensionless) time, $t\,\omega_{pi}$. At early times ($t\,\omega_{pi} <$ 200) the electric and magnetic field fluctuations grow at the same exponential rate and saturate at the same time. This behavior is expected and is quantitatively consistent with, linear theory. The waves that grow at early times are lower hybrid waves with frequency ω_{LH}.

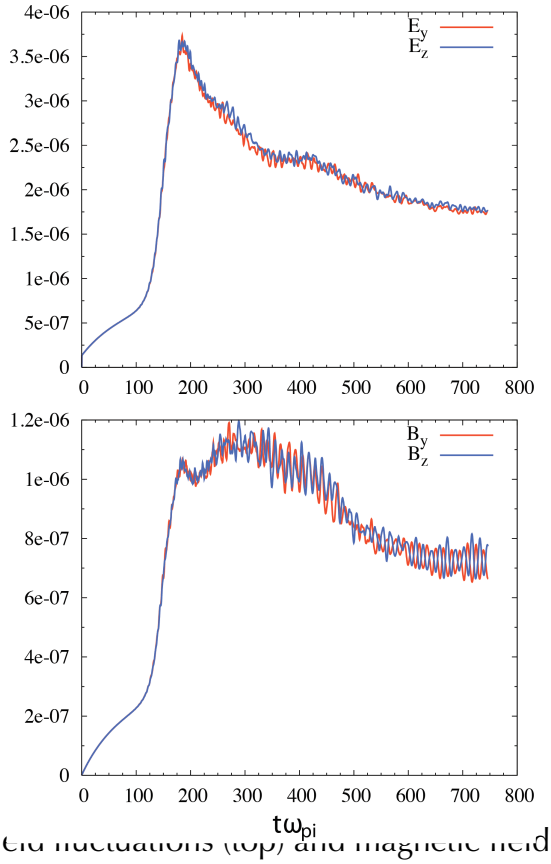

Figure 3.2.1 Electric field fluctuations (ω_p) and magnetic field fluctuations (bottom) as a function of time.

After the lower hybrid waves saturate ($t\,\omega_{pi} \approx 175$) the electric and magnetic field fluctuations behave differently. The electric field energy decays rapidly to a much lower level as it loses energy by heating the background plasma and ring ions. In the process the lower hybrid waves form density striations - regions of high and low background density that are aligned along the background magnetic field. These density striations are believed to be critical for conversion wave energy from the lower hybrid to the whistler modes [*Eliasson and Papadopoulos*, 2008]. Formation of density striations and wave-wave scattering in the striations are some of the processes that were also tested experimentally (section 3.3).

After the lower hybrid waves saturate, the electric field fluctuations decay. The decay is due to a quenching of the ring instability. The lower hybrid waves heat both the background plasma and the ring ions and as the ring ions heat the ring distribution becomes more stable the rate of extraction of energy in lower hybrid waves decreases.

In contrast to the electric field, the magnetic field fluctuations grow and persist at that level for an extended period of time. This corresponds to the development of whistlers waves. The ratio of electric and magnetic field fluctuations shows that they are

electromagnetic waves capable of propagating out into the radiation belts. It is these whistler waves that are analyzed in more detail to understand the amount of power in the waves, their direction of propagation, and the physics of the conversion process.

Plots such as these were analyzed to calculate the conversion efficiency from lower hybrid to whistler waves. The relative power was calculated by dividing the maximum power in the whistler wave magnetic field (δB_w^2) by the maximum power in the lower hybrid electric field (δE_{ES}^2). Referring to figure 3.2.1, the maximum electric field power, δE_{ES}^2, is taken at the peak in the top plot and δB_w^2 is taken at the peak in the bottom plot. The ratio of these to quantities is related to the maximum conversion efficiency.

Figure 3.2.2 plots the ratio of the magnetic (whistler) to electric (lower hybrid) fluctuations for a wide variety of simulation runs. The power ratio is plotted as a function of the simulation ion-to-electron mass ratio, m_i/m_e, for different simulation conditions. The full scale plot (on the left) shows results from both 2-dimensional simulations and 3-dimensional simulations. The 3D results are inherently more realistic (and more computationally intensive) but they also show qualitative differences from the 2D results.

In the first place the power ratios for the 2D simulations are generally higher, and sometimes much higher, than for the 3D simulations. We also see that in the 2D simulations (there is signifiant variation in the power ratio for different values of the background plasma β. In the 2D simulations the spread in the power ratio results for different β increases as a function of m_i/m_e and the power ratio can become quite large for high mass ratios and high β. These all appear to be artifacts of the reduced dimensionality of the simulation. According to theory the power ratio should be independent of the ion to electron mass ratio. We see that in 3-dimensions it is.

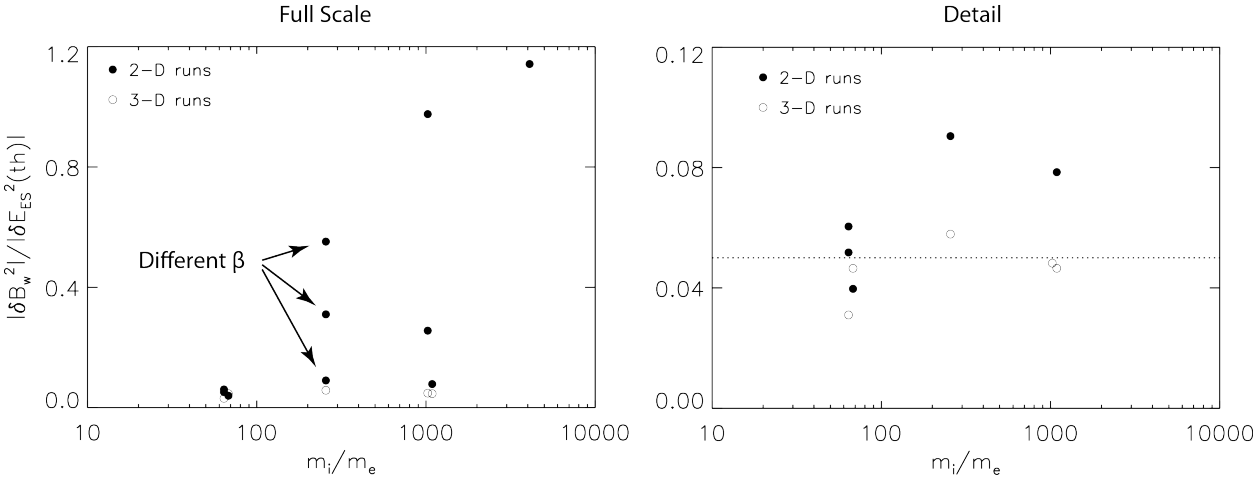

Figure 3.2.2 The ratio of the magnetic (whistler) to electric (lower hybrid) fluctuations for a wide variety of simulation runs

3.3 Summary of Results from the Laboratory Experiments

During the course of this investigation, we conducted a series of laboratory experiments using the Large Area Plasma Device (LAPD) at UCLA. The objective of the laboratory experiments was to verify that the PIC simulation results could be reproduced, to study wave conversion in a realistic environment, and to understand how the results of both the simulation and the experiments should be scaled to the conditions in space. We conducted three types of experiments. In the first set of experiments we injected lower hybrid waves directly into the plasma at moderate power. The second set of experiments used the same direct injection but studied the response as a function of injected power. This series also applied methods to limit the undesirable artifacts found in the first experiment. The third did not use and antenna. It used an ion beam from an accelerator to produce an ion ring distribution. The experiments were phased in order to produce preliminary results quickly and more and more refined results as equipment could be upgraded, purchased, or built for our experiments.

As with the PIC simulations, the objectives of the experiments was to study the partitioning of energy when ion ring distributions produce lower hybrid waves and the process by which lower hybrid waves can convert to whistler waves.

The LAPD facility is the largest basic plasma physics device in existence. It is a plasma chamber that is 1 m in diameter and 20 m long (figure 3.3.1). It is surrounded by magnets that produce a magnetic field aligned with the long axis of the chamber. These are seen as red and yellow disks in the picture. It is equipped with a large array of probes and sensors that can take exquisitely detailed measurements of the conditions at different points in the chamber

A 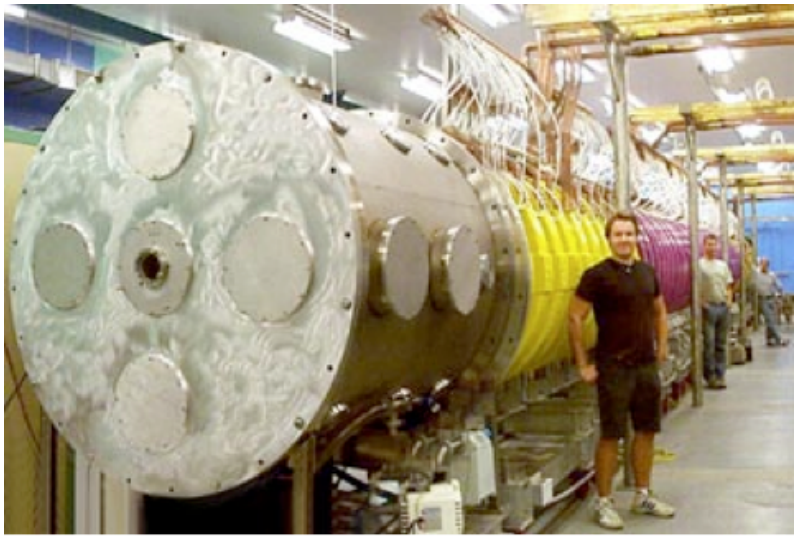 B 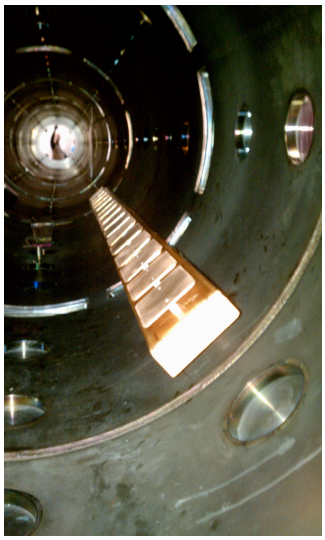

Figure 3.3.1 The LAPD chamber (A) and the antenna mounted inside (B)

Figure 3.3.2 shows the experimental configuration for the first and second set of experiments. The Z-axis is aligned along the axis of the chamber and is also the direction of the magnetic field, B. Waves are launched from an antenna mounted on the side of the chamber. Lower hybrid waves propagate, nearly perpendicular to B, into the center of the chamber. Data are collected by the probe arrays and typical collections (but not all) are done in planes perpendicular to B, i.e. X-Y planes. Data collections sufficiently far removed from the antenna in the Z direction are used to detect the presence of whistler waves that may be created by nonlinear conversion from lower hybrid waves.

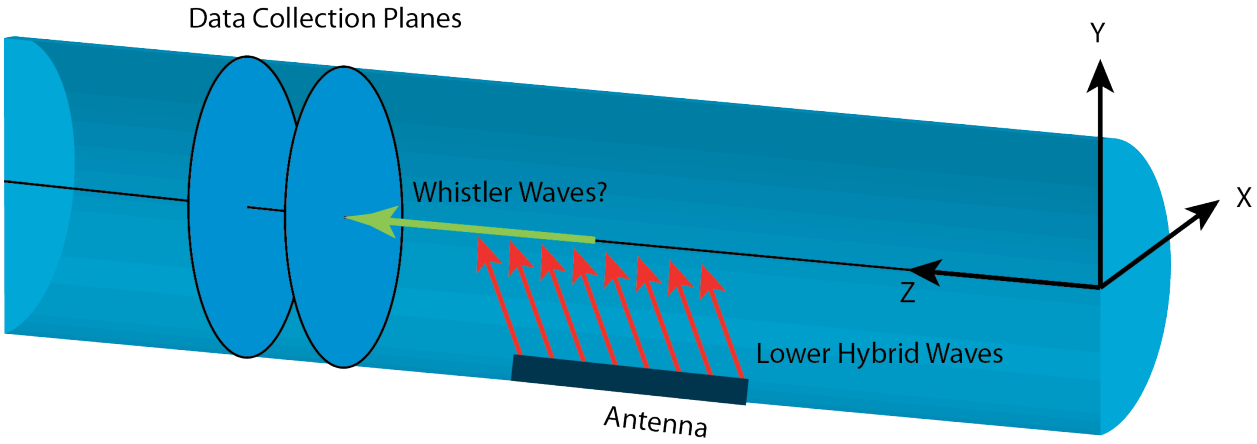

Figure 3.3.2 Schematic of the laboratory experiment.

The challenge with direct comparison of the experiment with simulations (or with conditions in the magnetosphere) lies in the fact that, even with petaflop computers, it is not possible for the simulations to reproduce the exact conditions in the laboratory (or in space). Therefore we use the standard scaling procedures. The physics of wave conversion are not directly dependent on parameters such as density, temperature, or magnetic field strength. Rather they are dependent on ratios of quantities that depend on these parameters. In particular the plasma beta, β, and the ratio of the plasma frequency to the gyro-frequency. Plasma beta, $\beta = P/P_B$, is defined as the ratio of the plasma pressure $P = nkT$ to the magnetic pressure $P_B = B^2/2\mu_o$, where T= temperature, n = density, B is the magnetic field strength, and k and μ_o are constants. The plasma and gyro-frequencies are characteristic frequencies of waves in a plasma and are defined, respectively, as $\omega_{pe} = (4\pi ne^2/m_e)^{1/2}$ and $\omega_{ce} = |e|B/m_e$ where e is the electron charge and m_e is the electron mass.

The conditions in the LAPD chamber scale to the same β and ω_{pe}/ω_{ce} as conditions in the Earth's magnetosphere. Preserving these ratios ensures that the physical processes in the experiments reproduce the same conditions that would be observed in the magnetosphere [*Gary*, 1993].

3.3.1 Experiment Phase 1: Medium Power Lower Hybrid Wave Injection

In phase 1 of our experiments, waves were launched from a 16-element antenna mounted on the lower side of the chamber (figure 3.3.1). As discussed in section 3.3, the presence of density gradients is thought to be an important requirement for conversion of lower hybrid to whistler waves. For sufficiently high powers of lower hybrid waves density depletions (and gradients) will be formed by the waves themselves as they bunch electrons in the plasma. In phase 1 the wave power launched from the antenna was moderate and probably not sufficient to create density depletions by itself. Normally in the LAPD, density increases smoothly from the sides of the chamber to a maximum on the central axis. Therefore, in phase 1, we imposed an artificial density depletion along the central axis of the chamber (the Z-axis) which is also aligned with the magnetic field, **B**. The density depletion was created by placing an absorbing disk (a mask) in front of the cathode that produces the plasma.

The lower hybrid waves propagate nearly perpendicular to the magnetic field going from the antenna into the center of the chamber where they encounter the plasma depletion. The lower hybrid waves propagate into the depletion where they can convert to whistler waves if the nominal scattering condition is satisfied [*Eliasson and Papadopoulos*, 2008].

The scattering condition is given by: $k_W = k_{LH} + 1/L$

where k is the wave number (inverse wavelength), the subscripts W and LH refer to whistler and lower hybrid, and L is the scale size of the depletion.

Phase 1 of our experiments produced ambiguous results. Whistler waves were observed at a downstream location (figure 3.3.2) at unexpectedly large amplitudes but the presence of those waves could be explained by either

- conversion of lower hybrid waves in the density depletion
- or, direct production of whistler waves by the antenna

In the case of conversion we could interpret the results as follows. The lower hybrid waves propagate from the antenna into the central density depletion. They nonlinearly convert into whistler waves at the same frequency and wave numbers that match the scattering condition. The whistlers then propagate nearly parallel to the magnetic field (along the axis of the chamber).

In the case of direct production the interpretation is different. We know from experience, simulation, and from direct measurement that the antenna produces both lower hybrid waves and whistler waves at the same frequency but with different directions of propagation. Ideally the power going directly into whistler waves would be negligible but in practice the whistler power is not negligible. In the conditions for Phase 1, the whistlers were also able to propagate away from the antenna and could propagate into the central

density depletion (but at a point much further downstream from the antenna). Once inside the density depletion the whistler waves are guided along the depletion in a manner similar to how light is guided along a fiber optic cable.

Both the detailed diagnostics in the Phase 1 experiment and the results from the Phase 2 and 3 experiments convince us that the whistler power observed in Phase 1 was primarily from direct production of whistler waves by the antenna. Any whistlers that were produced by nonlinear conversion from lower hybrid waves were at far too low a power to be observed in the presence of the directly-injected whistlers.

3.3.2 Experiment Phase 2: High Power Lower Hybrid Wave Injection

In Phase 2 of the LAPD experiments we modified the experiment in two ways. First, we increased the power supplied to the antenna to levels at which the lower hybrid waves naturally produce field-aligned density striations that are capable of satisfying the scattering condition. Second, we modified the plasma conditions to control the amount of whistler power that could propagate away from the antenna.

For this phase we varied the total power launched from the antenna from ~0 to over 200 Watts. We also reduced the total density in the chamber to a point where whistler waves injected directly from the antenna are absorbed before they can propagate into the center of the chamber.

We first measured the total wave power near the antenna where both whistler and lower hybrid waves should still be dominated by direct injection. The results are shown in figure 3.3.3. The plot of near-field wave power shows that the amount of measured wave power is proportional to the amount of injected power. The relationship is clearly linear and gives the amount of wave power launched into the plasma by the antenna. But, in the near field, it is not possible to separate whistler and lower hybrid wave power.

Figure 3.3.3 also shows the amount of wave power in the far-field, i.e. far downstream from the antenna in a region that is inaccessible to the lower hybrid waves. In the far-field, downstream region most of the power should be whistler power but the amount of directly injected whistler power in the far field should be very low under the plasma density conditions used in this phase of the experiment. We see that at low injected power the far-field wave power is indeed quite low. At about 60 W of antenna power the far-field wave power begins to increase. This is consistent with the onset of creation of density striations and non-linear conversion of lower hybrid waves into parallel-propagating whistler waves. At antenna powers somewhere around 400 W the amount of wave power in the far field begins to saturate (as expected from analytic theory and PIC simulations). In the saturated regime additional power only goes into heating of the plasma.

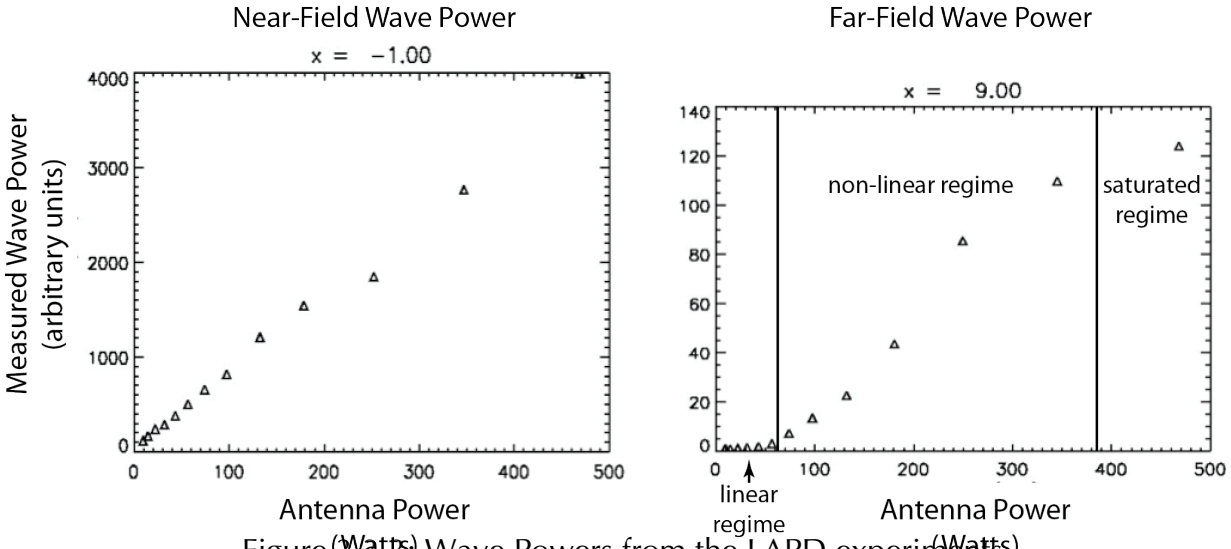

Figure 3.3.3: Wave Powers from the LAPD experiments.

A comparison of the near-field wave power and the far field wave power at the top of the non-linear regime gives an upper bound on the non-linear conversion from lower hybrid waves to whistler waves of 10^{-4}. (This value cannot be read directly off the graphs in figure 3.3.3 but is detailed in the attached UCLA-LAPD Report.)

The reason that these measurements give an upper bound on the conversion efficiency is that we assume all the wave power in the near field measurements are lower hybrid waves. In reality some power in the whistler mode directly from the antenna is almost certainly present in the near field before it is absorbed by the plasma.

As defined in section 3.1 the efficiency measured in this experiment is the conversion efficiency from lower hybrid to whistler waves, ε_W while the total efficiency of conversion of ring distribution energy to whistler energy is give by $\varepsilon = \varepsilon_{LH} \times \varepsilon_W$. With $\varepsilon_W < 10^{-4}$ the total efficiency, ε, cannot be larger than 10^{-4}, even if $\varepsilon_{LH} = 1$.

3.3.3 Experiment Phase 3: Ion Beam Injection

In phase 3 of the experiments we were able to eliminate the antenna as the source of lower hybrid waves (and contamination from directly-injected whistler waves). In phase 3 we injected an ion beam at one end of the chamber to produce an ion ring distribution very similar to a chemical release in space and to the initial conditions in the PIC simulations. In this case, it is the unstable ion ring distribution that is the source of lower hybrid waves, not an antenna.

The ion beam was injected at a small angle at the end of the chamber where the magnetic field is relatively weak. As the beam propagates into the main part of the chamber where the field is much stronger (and uniform) the pitch angle changes giving a ring distribution

with ion pitch angles in the 20°-50° range. Beam energies ranged from 10-20 kV with current densities up to 25 A/cm^2 giving total ion beam powers as high as 80 kW which is more than sufficient to generate strong lower hybrid wave turbulence and the same density striations that were produced in phase 2 with the high-power antenna.

Measurements confirmed that the ion ring distribution produced lower hybrid waves that were strongest in the center axis of the chamber, i.e. near the location of the ion beam. The amplitude of the lower hybrid waves grows very quickly to a saturation level and then remain fairly constant. The saturation of the lower hybrid wave power is given by the partitioning of energy in the instability. Some of the energy in the ion ring distribution goes into lower hybrid waves. Some of the energy in the ion ring distribution goes into heating the background plasma. Some of the energy goes into heating of the ring ions themselves. When the ring ions reach a certain temperature the ring distribution is no longer unstable and no new wave energy can be extracted.

As in earlier phases of the experiment, whistler energy was measured downstream of the location of the beam and the beam-generated lower hybrid waves. This ensures that the waves measured downstream are propagating, electromagnetic, whistler waves. The total power measured was < 2 mW.

Phase 3 of our experiments directly measured the conversion efficiency from ion ring power to whistler wave power, $\varepsilon = \varepsilon_{LH} \times \varepsilon_{W}$. The result is that $\varepsilon < 10^{-6}$ (and perhaps much less) which, again, is in good agreement with the PIC simulation results of and far below previous estimates.

3.4 Reverse Engineering; How Much Whistler Power is Needed?

Ultimately, to test a remediation scheme it is also important to know the efficiency of the scattering of HANE electrons by whistler waves. The majority of the work done under this project was done to evaluate the efficiency of chemical release remediation and the efficiency of the conversion of ion kinetic energy to lower hybrid wave energy to whistler wave energy. Since we found that efficiency to be impractically low, the question of scattering efficiency might seem to be moot.

Chemical release is not, however, the only way to produce whistler waves in space. There are other schemes to inject whistler wave power from ground-based antennas, inject whistler power from space-based antennas, and other novel schemes to generate whistler waves in space without antennas (or conversion of wave modes).

Therefore, we also investigated the so-called “reverse engineering” approach. In this approach we attempted to answer the question How much whistler power is needed to remediate a given HANE belt in a given amount of time. Due to termination of the project this work did not progress as far as we would have hoped but preliminary results were very encouraging. It does not take terra watts of wave power to remediate scenarios of

interest which means that practical remediation systems based on direct whistler generation may be feasible.

We first need to establish a baseline for what we mean by “remediation”. It is never possible to get rid of all the electrons from a HANE since the decay is exponential. Similarly, a definition based on getting fluxes down to “background” level depends on the background level chosen and whether remediation of the natural electron fluxes is included in the calculation.

We established a quantifiable criteria for remediation based on the effect on a satellite. We define the remediation target to be that the total dose from a HANE in a given time, Tr, is equal to the total dose that the satellite would receive from the natural belts in a year. Effectively this means that, given a remediation wave power, Pr, that acts for a time, Tr, the lifetime of a satellite is reduced by approximately 1 year relative to it’s design lifetime. A different target dose could be chosen and the results should scale approximately linearly - e.g. a target of 6-months reduction of satellite lifetime would require twice as much remediation wave power.

To do this calculation we start with a particular HANE scenario and calculate the initial HANE belt using the DREAM Electron Source Model (ESM). We use the DREAM 3-dimensional radiation belt diffusion model to calculate the effect on the HANE belt from whistler waves of a given power and duration. In the case shown schematically in figure 3.4.1 we ran the ESM for a 1 Mt HANE at a height of 400 km at latitudes corresponding to L = 1-3. The 3D diffusion code calculates the evolving pitch angle distribution and the orbit propagator (fly-through tool) calculates the dose rate on a LEO satellite at 1 km altitude.

The next step is to calculate the natural dose accumulated by a given satellite over one year. For this example we chose the Globalstar satellite. We calculate the range of L-shells spanned by the HANE belt, distribute power over that volume and let it act on the HANE belt. Figure 3.4.2 shows the total amount of wave power and the total amount of time the wave power needs to be applied in order for the HANE dose on the Globalstar satellite during that time to equal the total natural dose received in a year.

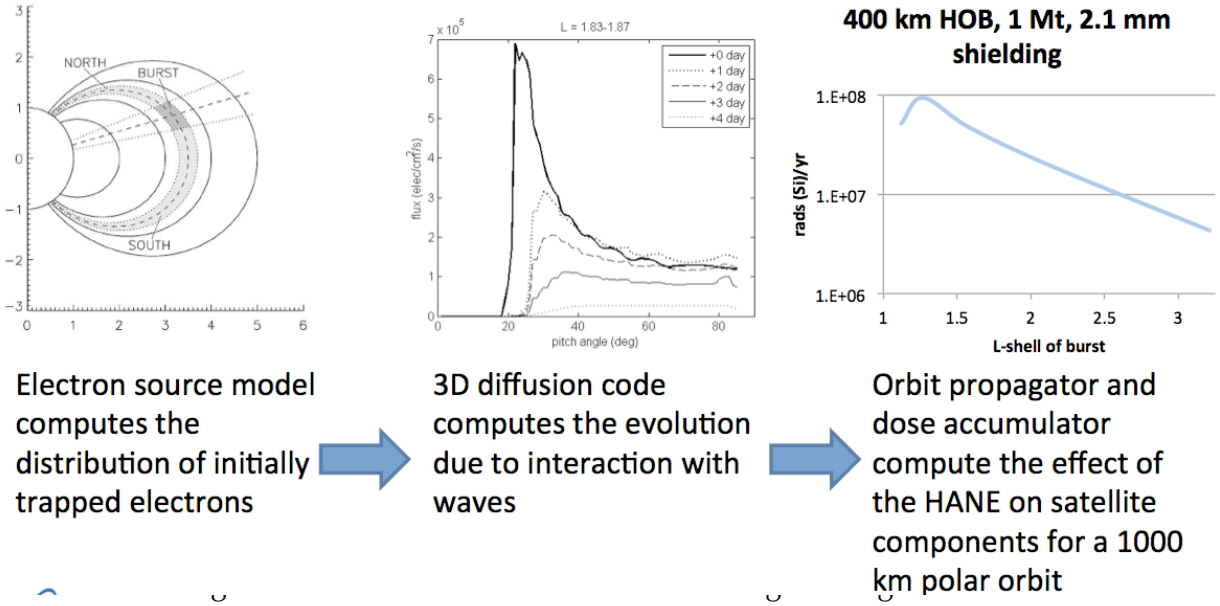

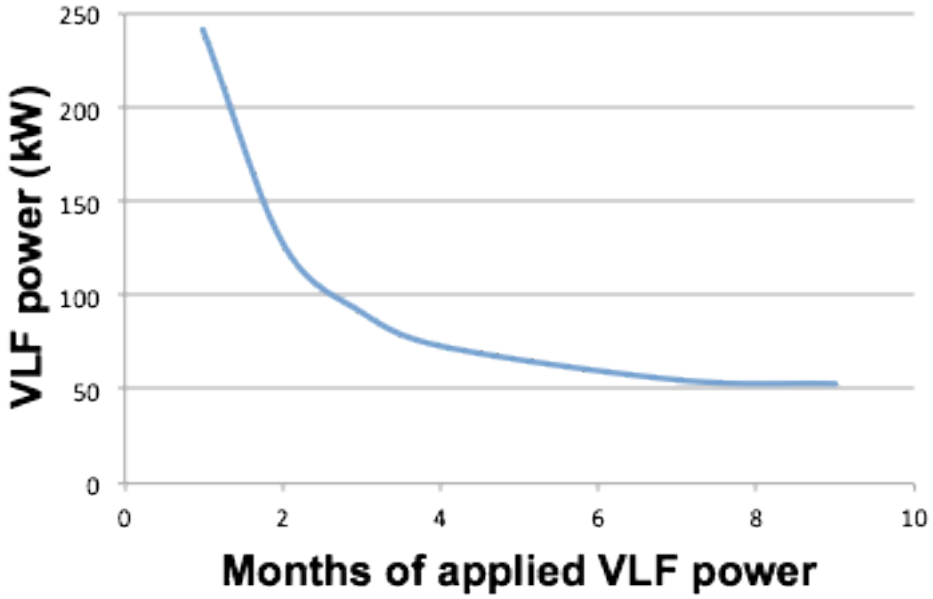

Figure 3.4.2 VLF Wave power (kW) as a function of time to hit the remediation target.

Naturally, the less time the wave power is applied the more power is needed. If wave power can be injected continuously for 3 months then the injected power needs to be approximately 100 kW. For an injected power of 50 kW the waves need to be injected continuously for more than 6 months. This metric can be used for an arbitrary target remediation time with more power required for shorter remediation times. In all cases,

points on this line give a dose that shortens a satellite's lifetime by approximately 1 year relative to the lifetime it would have had in the absence of a HANE.

We caution, that the "reverse engineering" calculations included here are preliminary but they do provide some important insights and ballpark engineering constraints.

For example, these results show that continuous wave injection is much more efficient than a single, pulsed injection of wave power. The whistler waves need to be present for sufficiently long times that they can interact with the electrons as they undergo their bounce and drift motion. However, if a system can be designed to sustain the presence of VLF whistler waves then the required powers are not unreasonable and practical remediation systems may be within technological reach.

Bibliography

Blake, J. B., et al. (1992), Injection of electrons and protons with energies of tens of MeV into L<3 on 24 March 1991, *Geophys. Res. Lett.*, *19*.

Eliasson, B., and K. Papadopoulos (2008), Numerical study of mode conversion between lower hybrid and whistler waves on short-scale density striations, *Journal of Geophysical Research*, *113*, A9, doi:10.1029/2008ja013261.

Friedel, R. H. W., et al. (2002), Relativistic electron dynamics in the inner magnetosphere: A review, *J. Atmos. Solar-Terrestrial Phys.*, *64*, 2.

Gary, S. P. (1993), *Theory of Space Microinstabilities*, Cambridge University Press, New York.

Millan, R. M., and R. M. Thorne (2007), Review of radiation belt relativistic electron loss, *J. Atmos. Solar Terr. Phys.*, *69*.

Mithaiwala, M., et al. (2011), Weak turbulence theory of the nonlinear evolution of the ion ring distribution, *Phys Plasmas*, *18*, 5, doi:Artn 055710

Doi 10.1063/1.3574389.

Reeves, G. D., et al. (2009), New directions for radiation belt research, *Space Weather*, *7*, S07004, doi:10.1029/2008SW000436.

Summers, D., et al. (1998), Relativistic theory of wave-particle resonant diffusion with application to electron acceleration in the magnetosphere, *Journal of Geophysical Research*, *103*, A9, doi:10.1029/98JA01740.